Ion Transport and Inhibitor Binding by human NHE1: Insights from Molecular Dynamics Simulations and Free Energy Calculations

*Nehad S El Salamouni,[†, ‡] Benjamin J. Buckley[†, ‡] Richmond Lee, [†, ‡] Marie Ranson,[†, ‡] Michael J. Kelso[†, ‡] and Haibo Yu,[†, ‡,]**

[†]School of Chemistry and Molecular Bioscience, University of Wollongong, NSW 2522, Australia.

[‡]Molecular Horizons, University of Wollongong, Wollongong, NSW 2522, Australia.

KEYWORDS

Na^+/H^+ exchanger 1, selectivity, MD simulations, FEP, PMF, amiloride, cariporide

ABSTRACT

The human Na^+/H^+ exchanger one (*h*NHE1) plays a crucial role in maintaining intracellular pH by regulating the electroneutral exchange of a single intracellular H^+ for one extracellular Na^+ across the plasma membrane. Understanding the molecular mechanisms governing ion transport and the binding of inhibitors is of importance in the development of anticancer therapeutics targeting *h*NHE1. In this context, we performed molecular dynamics (MD) simulations based on the recent cryo-electron microscopy (cryo-EM) structures of outward and inward-facing conformations of *h*NHE1. These simulations allowed us to explore the dynamics of the protein, examine the ion-translocation pore and confirm that Asp267 is the ion-binding residue. Our free energy calculations suggest that Na^+ and K^+ bind similarly at the ion-binding site. Consequently, Na^+ over K^+ selectivity cannot be solely explained by differences in ion binding. Our MD simulations involving *h*NHE1 inhibitors (cariporide and amiloride analogues), showed maintained stable interactions with Asp267 and Glu346. Our study highlights the importance of the salt bridge between the positively charged acylguanidine moiety and Asp267, which appears to play a role in the competitive inhibitory mechanism for this class of inhibitors. Our computational study provides a detailed mechanistic interpretation of experimental data and serves the basis of future structure-based inhibitor design.

INTRODUCTION

Na^+/H^+ exchangers (NHEs) are vital for controlling the intracellular pH by shuffling protons (H^+) across the cellular membranes in exchange for monovalent cations, such as sodium (Na^+), lithium (Li^+) and potassium (K^+).[1, 2] There are 10 isoforms of NHEs (NHE1 - NHE10).[1, 3] *h*NHE1 (the human form of NHE1) is a ubiquitously expressed integral transmembrane (TM) glycoprotein present in all cells. It controls the electroneutral exchange of a single intracellular H^+ for an extracellular Na^+ ion (1:1 stoichiometry) across the plasma membrane, acting to elevate intracellular pH (pH_i). *h*NHE1 thus regulates Na^+ levels, pH_i,[4] cell volume,[4-6] proliferation[4] and cell migration.[7, 8] and has been correlated with pathological conditions such as heart disease[9-11] and hypertension.[12, 13] In cancer cells, elevated *h*NHE1 activity enhances malignant transformation,[14] invasion and metastasis.[15, 16] *h*NHE1 has been implicated in cancer regulation,[17] progression and metastasis of breast,[15, 18-20] ovarian,[21, 22] pancreatic,[23, 24] gastric[25] and prostate[26] cancers as well as hepatocellular carcinoma.[27]

The existence of cation/H^+ exchangers was first proposed in 1961.[28] In 1976, the Na^+/H^+ antiport system was studied in rat intestinal and renal brush-border membranes.[29] In 1989, the complete sequence of *h*NHE1 was identified.[30] *h*NHE1 comprises 815 amino acids that form two domains: 1) N-terminal hydrophobic domain that comprises 500 amino acids, as well as membrane-associated segments (intracellular and extracellular loops). It is responsible for ion transport, pH sensing and amiloride binding. This domain contains three N-glycosylation sites at Asn75, Asn370 and Asn410[30, 31] 2) C-terminal intracellular cytosolic domain. The C-terminal domain is highly hydrophilic, having a net positive charge and bears a number of phosphorylation sites.[30] It regulates the ion-exchange activity[32] following phosphorylation or interactions with intracellular

signaling molecules.[32, 33] *h*NHE1 exists as a dimer[34] and has two states; an inward-facing state which is open to the inside of the cell and an outward-facing state that is open to the extracellular environment.

Until mid-2021, a complete three-dimensional structure of *h*NHE1 had not been described.[34] The only reported experimental structures were of some bacterial and archaeal Na^+/H^+ antiporters, such as the NhaA of *Escherichia coli* (*Ec*NhaA),[35] NapA of *Thermus thermophilus* (*Tt*NapA),[36] NhaP1 of *Methanocaldoccocus jannaschii* (*Mj*NhaP1)[37] and NhaP of *Pyrococcus abyssi* (*Pa*NhaP).[38] For *h*NHE1, nuclear magnetic resonance (NMR) structures had been reported for isolated TM segments TM4 (PDB ID: 1Y4E),[39] TM5 (PDB ID: 2L0E),[40] TM7 (PDB ID: 2HTG),[41] TM6-TM7 (PDB ID: 2MDF),[42] TM9 (PDB ID: 2K3C),[43] TM11 (PDB ID: 2KBV)[44] and IL5 (PDB ID: 6BJF)[45] at the outset of this project. Several attempts had been made to build a three-dimensional model of *h*NHE1 and a number of topology models had also been proposed in literature.[46-49] The first, based on hydropathy analysis of *h*NHE1 applying the Kyte-Doolittle algorithm, suggested 10 - 12 TM segments.[50] Wakabayashi *et al.* later developed a model based on cysteine scanning accessibility studies of 83 residues that suggested 12 TM segments with residues 1 - 127 forming two TM segments and residues 315 - 411 comprising TM9 and a large extracellular loop (EL5) (**Figure S1**).[46] Landau *et al.* then proposed a model that was based on homology modeling with the *Ec*NhaA (15% identical and 31% similar to *h*NHE1)[47] which was in agreement with the mutagenesis studies on various residues.[47] This model also proposed 12 TM segments but with residues 1 - 127 cleaved as a signal sequence and thus absent in the mature protein (**Figure S1**). The second striking difference from the model of Wakabayashi *et al.* was in the region comprising residues 315 - 411. They proposed that this region formed three TM segments (TM7, TM8 and TM9) rather than a single TM9 and EL5. Nygaard's model was based

on homology with *Ec*NhaA[48] as well as electron paramagnetic resonance analyses while also considering previous experimental cysteine accessibility studies.[46] The latest model by Dutta *et al.* was based on pairwise sequence alignment with *Mj*NhaP1 (20% identical and 38% similar to *h*NHE1) and homology modelling using the same structure. They performed manual adjustments to their model to place the biochemically extracellular accessible residues on the outer side in order to align with the experimental data.[49] TM segment assignments in the models by Nygaard *et al.* and Dutta *et al.* were similar to Wakabayashi's model.

Recently complete structures of *h*NHE1 in complex with calcineurin B-homologous protein 1 (CHP1) in the outward (PDB ID: 7DSX; 3.5 Å) and inward-facing (PDB ID: 7DSW; 3.3 Å) states, derived from cryo-electron microscopy data, were reported.[34] CHP1 is an obligate binding partner that promotes the biosynthetic maturation, cell surface expression and pH-sensitivity of *h*NHE1. These structures confirmed that *h*NHE1 comprises 13 TM helices and residues between 329 and 371 form two TM segments (TM8 and TM9) and the previously assigned extracellular loop 5 (EL5) as TM10 (**Figure S2**). The outward-facing structure of *h*NHE1 (PDB ID: 7DSX; 3.5 Å)[34] has bound cariporide, which binds to the extracellular side of *h*NHE1 forming a key salt bridge with Asp267, hydrogen bonds to Glu346, parallel cation−π and T-shaped π−π interactions with the sidechain of Phe162 (**Figure S2**). The methylsulfonyl group of cariporide is buried within a sub-pocket formed by Asp159, Leu163, Asp95, His98, and Val99, consistent with a previous observation that small moieties commonly occupy this position in most *h*NHE1 specific inhibitors. In particular, mutations of Leu163 reduce inhibitor sensitivity in *h*NHE1.[51] Since the residues involved in cariporide binding are from both the core and dimerization domains, it has been speculated that cariporide inhibits the *h*NHE1 activity mainly by blocking the relative sliding movement between the two domains in addition to competing with Na^+ for the extracellular

substrate-binding site. Cariporide is the first known and best studied specific and selective *h*NHE1 inhibitor.[52]

Another class of *h*NHE1 inhibitors include the pyrazinoylguanidine-type inhibitors (amiloride and its derivatives).[53, 54] Amiloride is a potent competitive *h*NHE1 inhibitor that has been proposed to displace extracellular Na^+ and possibly Li^+, preventing it from binding to the ion transport site of *h*NHE1.[51, 55, 56] Some mutations reported significant effects on the inhibitor resistance associated with effects or no effects on Na^+ affinity, which suggested that their binding sites might be adjacent.[51, 57-59] The introduction of alkyl substituents to the amine nitrogen at the 5-position of amiloride improved the inhibitory potency against *h*NHE1.[57, 60] 6-Substituted amiloride analogues displayed nanomolar potency against *h*NHE1.[61]

Although the transport of K^+ through plasma membrane NHEs is not detectable, it has been observed that K^+ can have a minor inhibitory impact on the activity of NHE1, thereby interfering to some extent with Na^+ transport.[1] *Mj*NhaP1,[62] *Pa*NhaP,[38] *Ec*NhaA,[35, 63, 64] and *Tt*NapA[36] are known to be selective for Na^+ over K^+. A previous computational study revealed that the inward-facing state of *Mj*NhaP1 favoured the binding of Na^+ over K^+ while the outward-facing state showed a weaker preference for Na^+.[62] Another study on *Ec*NhaA suggested that differences in ion-binding are not a sufficient determinant of selectivity and that selectivity is determined at a later stage of the transport cycle.[65] In contrast, it has been reported that NHEs present in intracellular compartments are capable of transporting cytosolic K^+.[1] *h*NHE8, yeast *Sc*NHX1 and plant *At*NHX1 are known to transport both Na^+ and K^+.[66-69] The selectivity and function of NHEs can be influenced by various factors, including vesicular curvature, lipid composition, ion gradients, and the surrounding environment.[1] These factors can significantly differ between intracellular compartments and the plasma membrane.[1]

Our previous work focused on the selective optimisation of the side-activities of amiloride and its analogues as anticancer agents.[54, 70-73] It has been reported that *h*NHE1 is among the potential targets for the observed anti-cancer effects of amiloride and its analogues.[54, 57, 60, 61] To begin, we constructed a three-dimensional homology model of *h*NHE1. With the publication of a long-awaited experimental structure and our interest in developing novel *h*NHE1 inhibitors, we subsequently conducted molecular dynamics (MD) simulations of both the apo and ligand-bound states. This enabled us to investigate the dynamics of *h*NHE1 and how it interacts with ligands. The potential of mean forces (PMFs) for Na^+ and K^+ ions along the ion-translocation pore and free energy perturbation (FEP) at the proposed ion-binding site were used to explore the differences in ion-binding and understand the molecular mechanisms for Na^+ over K^+ selectivity. We mainly focus on the results of simulations based on the cryo-EM structures. Simulations based on homology modeling were broadly consistent with those based on cryo-EM structures and are included in the **Supporting Information section**.

METHODS

Molecular Dynamics Simulations

Alignments of the outward and inward-facing states of the protein models within the lipid bilayer were conducted using OPM (Orientations of Proteins in Membranes database) online server.[74] CHARMM-GUI Membrane Builder was used to build the protein membrane complexes.[75-77] Proteins were embedded in a 1-palmitoyl-2-oleoyl-sn-glycero-3-phosphocholine (POPC) lipid bilayer with 276 POPC lipid molecules (140 for the top periplasm-facing leaflet and 136 for the

bottom cytoplasm-facing one) using the replacement method. The systems were solvated using TIP3 water molecules that extended for 15 Å on both sides of lipid bilayer and neutralized with Na^+ and Cl^- counter ions to achieve a salt concentration of 0.15 M. The systems were in a 117 Å × 117 Å × 115 Å tetragonal box. The systems were minimised and equilibrated following consecutive equilibration runs (1 ns each) during which the restraints were gradually reduced (see **Table S1** for more details about restraints). Three different types of restraints were applied: 1) Positional harmonic restraints for protein backbone and side chain heavy atoms and for Na^+ and Cl^- ions; 2) Repulsive planar restraints for water molecules to prevent them from entering the membrane hydrophobic region; 3) Planar restraints for membrane head groups to hold them in position along the *z*-axis. This was followed by production runs with no restraints using NAMD 2.14[78] and CHARMM36m force field.[79, 80] Ligand parameters were created using the CHARMM General Force Field (CGenFF) generated by the ParamChem server (https://cgenff.umaryland.edu).[81] PROPKA was used to identify the protonation states of the protein ionisable residues[82] which were simulated in their default protonation states. Constant temperature (310.15 K) was maintained by applying Langevin dynamics with damping coefficient of 1.0 ps^{-1} and constant pressure (1 atm) by Langevin Piston Nose-Hoover method applying a piston period of 50 fs and piston decay of 25 fs. Particle Mesh Ewald (PME) algorithm was applied to treat the long-range electrostatic interactions with a 12 Å cutoff distance to treat non-bonded interactions. Bonds involving hydrogen atoms were kept rigid with SETTLE.[83] A time step of 2 fs was used, and snapshots were saved every 500 steps. For the apostates, six independent simulations 400 ns each of the outward and inward-facing states were performed. After 100 ns a bound Na^+ was replaced by K^+ and simulations were run for 300 ns. For the ligand bound states, six independent simulations 400 ns each were performed. The atomic positional root-mean-square

deviation (RMSD) and the atomic positional root-mean-square fluctuations (RMSF) with respect to starting structures were calculated to monitor the global properties of the structural evolution during the simulations. VMD 1.9.4 was used for visualisation of trajectories and analysis of simulations.[84] HOLE program was used for visualization and analysis of the pore dimensions.[85] Hydrogen bond analysis was performed using VMD with donor-acceptor distance cutoff of 3.0 Å and donor-hydrogen-acceptor angle cutoff of 20°. A summary of the simulated systems is provided in **Table S2**.

Steered Molecular Dynamics (SMD)

To explore the ion transport pathway, Na^+ the SMD atom, was pulled along the *z*-direction with a constant velocity of 20 Å/ns and a force constant of 5 kcal/mol/Å^2. Two SMD systems were constructed with two different Na^+ starting positions. The first involved pulling a Na^+ from the outside of the protein until it was bound to the proposed ion-binding Asp267 residue in the outward-facing state of *h*NHE1 and the second pulling a Na^+ bound to Asp267 in the inward-facing state until it reached the inner side of the protein. Equilibrated systems from MD simulations were used as starting points for the SMD simulations. To prevent the protein or the entire system from drifting under the applied force, positional restraints with a force constant of 5 kcal/mol/Å^2 was applied to alpha carbon (C_α) atoms of peripheral protein residues Pro102, Ile146, Gly294, Phe348 and Asn410. Simulation of each system was performed (each lasted 1 ns) using similar parameters to the MD simulations.

Potential of Mean Force (PMF) Calculations

From the SMD simulations and along the ion-translocation axis of the outward and inward-facing states, 23 umbrella windows were generated at 1 Å interval for each, respectively. A force constant of 2.5 kcal/mol/Å^2 was applied to restrain the ions in each umbrella window. Each window was simulated for 24 ns to ensure the convergence of the PMF calculation. Weighted Histogram Analysis Method (WHAM) was used to construct the unbiased PMF.[86]

Alchemical Free Energy Perturbations (FEP)

Free energy differences for the binding of Na^+ and K^+ to the proposed ion-binding residue Asp267 in the outward and inward-facing states of *h*NHE1 were calculated using alchemical FEP calculations. In these simulations, a Na^+ bound to Asp267 was perturbed to a K^+ in the outward and inward-facing states and in bulk water. These alchemical transformations were performed with the dual topology scheme using 20 equally distributed λ windows between 0 and 1 (0.0, 0.05, 0.1, ..., 0.9, 0.95, 1.0), bidirectionally (*i.e.* forward and backward simulations). Weak harmonic restraints with force constants of 1.0 kcal mol^{-1} Å^{-2} were placed on the perturbed ions to maintain the ion bound to Asp267. To prevent numerical instabilities as ions were created or destroyed, a soft-core potential was used with alchVdWShiftCoeff = 4.0. Initial 1.0 ns equilibration simulations were carried out for each system, including 1,000 minimisation steps followed by 10.0 ns of production runs. ParseFEP plugin 2.0[87] within VMD 1.9.4 was used to compute the free energy differences as well as estimate the statistical error where the forward and backward simulations were combined using the Bennett acceptance ratio (BAR) estimator.[88]

Molecular Docking

Docking was performed using Autodock Vina package 1.2.0.[89, 90] Structures were first prepared and optimized using ChemDraw 20.1 and Avogadro 1.2.0.[91] The acylguanidine moiety was protonated for all inhibitors. AutoDockTools 1.5.6[92, 93] was used to assign rigid and rotatable bonds and to remove non-polar hydrogens. Docking was performed in a 20 Å × 20 Å × 20 Å box centred at the inhibitor binding site of *h*NHE1. An exhaustiveness number of 64 was applied.

RESULTS AND DISCUSSION

Homology modeling of the *h*NHE1

At the start of this work, a complete characterization of the structure for *h*NHE1 was not yet available. Therefore, our goal was to create a homology model of *h*NHE1 (**Table S3**) by leveraging multiple sequence alignment (**Figure S3**) based on the closely related antiporter *Mj*NhaP1. With the release of a cryo-EM structure of *h*NHE1, we were able to directly compare our model with the experimental model. Additional information regarding the creation of our homology models for *h*NHE1 can be found in Supporting Information (**Figures S3** – **S9** and **Tables S3** and **S4**).

While previous models proposed a 12 TM structure of *h*NHE1, we propose 13 TM segments. The recent cryo-EM structure of *h*NHE1 included residues 59 to 590 arranged as 13 TM helices.[34] In our model, TM1, TM2, TM3, TM7, TM8, TM9, TM10 constitute the dimerization domain while TM4, TM5, TM6, TM11, TM12, TM13 constitute the ion transporting domain (**Figure S4**), which is consistent with the latest cryo-EM structure.[34] Only a few differences between the assignment of the beginning and ending residues forming each TM segment between our model and the recent structure of *h*NHE1 (**Table S4)**. The ColabFold[94] implementation of AlphaFold2[95] was also used

to predict the structure of *h*NHE1, which adopted the inward-facing state. A schematic diagram of our homology model with a comparison to all others is illustrated in **Figure 1**. The superimposed outward-facing state of the experimental (PDB ID: 7DSX) structure with the homology model and its MD equilibrated structure have RMSD values of 5.1 and 5.3 Å, respectively. Structures of the experimental inward-facing state (PDB ID: 7DSW) superimposed with the homology and its MD equilibrated structure have RMSD values of 5.0 and 5.5 Å, respectively. The inward-facing state predicted by AlphaFold2 displayed a lower RMSD of 1.2 Å compared to its respective cryo-EM structure (PDB ID: 7DSW) (**Figure S5**).

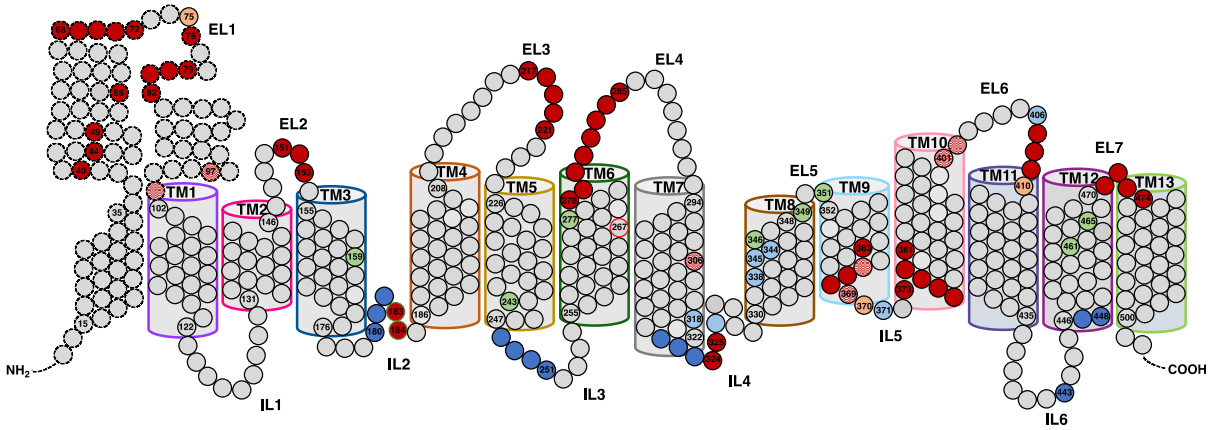

Wakabayashi	1	2	3	4	5	6	7	8		9	EL5	10	11	12
Nygaard	1	2	3	4	5	6	7	8		9	EL5	10	11	12
Dutta	1	2	3	4	5	6	7	8		9	EL5	10	11	12
Landau			1	2	3	4	5	6	7	8	9	10	11	12
El Salamouni		1	2	3	4	5	6	7	8	9	10	11	12	13
Cryo-EM		1	2	3	4	5	6	7	8	9	10	11	12	13
Alphafold		1	2	3	4	5	6	7	8	9	10	11	12	13

Figure 1. Schematic diagram of our homology model of *h*NHE1 showing the 13 TM helical domains (TM1 to TM13). Residues 15 to 101, which had no structural template, are absent in the model (dotted circles). Residues found to be extracellularly accessible in cysteine accessibility studies are shown as red circles, while intracellularly accessible residues are blue (residues identified in the work by Wakabayashi *et al*. experiments are dark blue[46] and those identified by

Liu *et al*. are lighter blue.[96] Residues that are known to be pore lining are drawn as green circles. The putative ion-binding Asp267 is outlined in red. N-glycosylation sites at Asn75, Asn370 and Asn410 are outlined in orange. Assignments of TM segments of all models are shown here and summarised in **Table S4**.

Ion binding to Asp267 in MD simulations of the cryo-EM structures of *h*NHE1

To gain insights of ion binding to *h*NHE1, we performed MD simulations of the outward and inward-facing states with Na^+ or K^+ with a total of 2.4 μs for each ion (**Table S2**). All simulations started with no Na^+ or K^+ bound to the proposed ion-binding residue Asp267.[34, 47] Simulations showed stable RMSD around 1.5 and 2.5 Å for the outward-facing states and 2.5 and 4.0 Å for the inward-facing states (**Figure S10**). RMSF plots revealed high fluctuations of the C_α atoms of residues in the regions comprising the loops and the regions of the assigned TM helices were rigid (**Figure S11**). Persistent ion binding and unbinding to the experimentally proposed ion-binding Asp267 were observed in the outward and inward-facing states (**Figure S12**).

No free energy differences for ion binding to Asp267

Asp267 is strictly conserved and proposed to be the ion-binding residue.[34, 47] The recent structure of *h*NHE1 suggests the side chain hydroxyl of Ser263, Asp267, the main chain of Val237 and a water molecule are involved in ion binding in the inward-facing state.[34] To investigate ion selectivity, we calculated the free energy differences for Na^+ and K^+ at the experimentally proposed binding site in the outward and inward-facing states according to the thermodynamic cycle outlined in **Figure S13**.

In these calculations, Na^+ was alchemically perturbed to K^+ in the outward and inward-facing states as well as in bulk. Free energy differences of 18.8 ± 0.1 and 17.9 ± 0.1 kcal/mol in the outward and inward-facing states were obtained, respectively. In the bulk, free energy change was 18.5 ± 0.03 kcal/mol, close to the value of 18.459 ± 0.002 kcal/mol previously reported.[62] Accordingly, at the ion-binding site, small free energy differences of + 0.3 ± 0.1 and – 0.6 ± 0.1 kcal/mol were observed for the outward and inward-facing states, respectively (**Figure S13**). Our calculations suggest that *h*NHE1 doesn't show a significant preference for the binding of either Na^+ or K^+ at the ion-binding site. To further investigate the reason for the Na^+ over K^+ selectivity, we calculated the free energy change of both ions along the pore in the outward and inward-facing states.

Free energy change of ions across the membrane

To explore the ion transport pathway and selectivity across the *h*NHE1, free energy profiles for Na^+ and K^+ along the *z*-axis of the outward and inward-facing states were constructed using umbrella sampling simulations (**Figure 2**). Cumulative data analysis was performed to monitor the convergence (**Figure S14**). Oxygen coordination numbers for Na^+ and K^+ along the pore were plotted to correlate with the observed free energy profiles (**Figure 2**).

In the outward-facing state, PMF profiles for both Na^+ and K^+ generally display similar shapes with a minor barrier to reach the free energy minima at ~ z = –10 Å, where both ions coordinate the side chain carbonyls of Asp267 and Glu346 in the outward-facing state, as evident from the plot of ion coordination numbers (**Figure 3**). This is consistent with previous data showing that Asp267 and Glu346 coordinate Na^+ during ion translocation.[34, 72, 97] In the inward facing state, to leave the ion-binding site and the embrace of the Asp267 and Glu346 side chains and pass further

to the intracellular side, Na^+ and K^+ overcome a free energy barrier of 5.8 kcal/mol and 6.6 kcal/mol, respectively (**Figure 2**).

The number of coordinating water molecules and total coordination numbers display small variation as both ions move from the bulk to the ion-binding site ($z < -10$ Å) (**Figure 3**). Following that, while both ions move from the ion-binding site to the inside ($z > -10$ Å) the number of coordinating water molecules decrease for from 5.5 to 4 in case of Na^+ and from 6 to 4.5 in case of K^+. Total coordinating oxygens decrease from 5.5 to 4 for Na^+ and 6 to 4.5 for K^+.

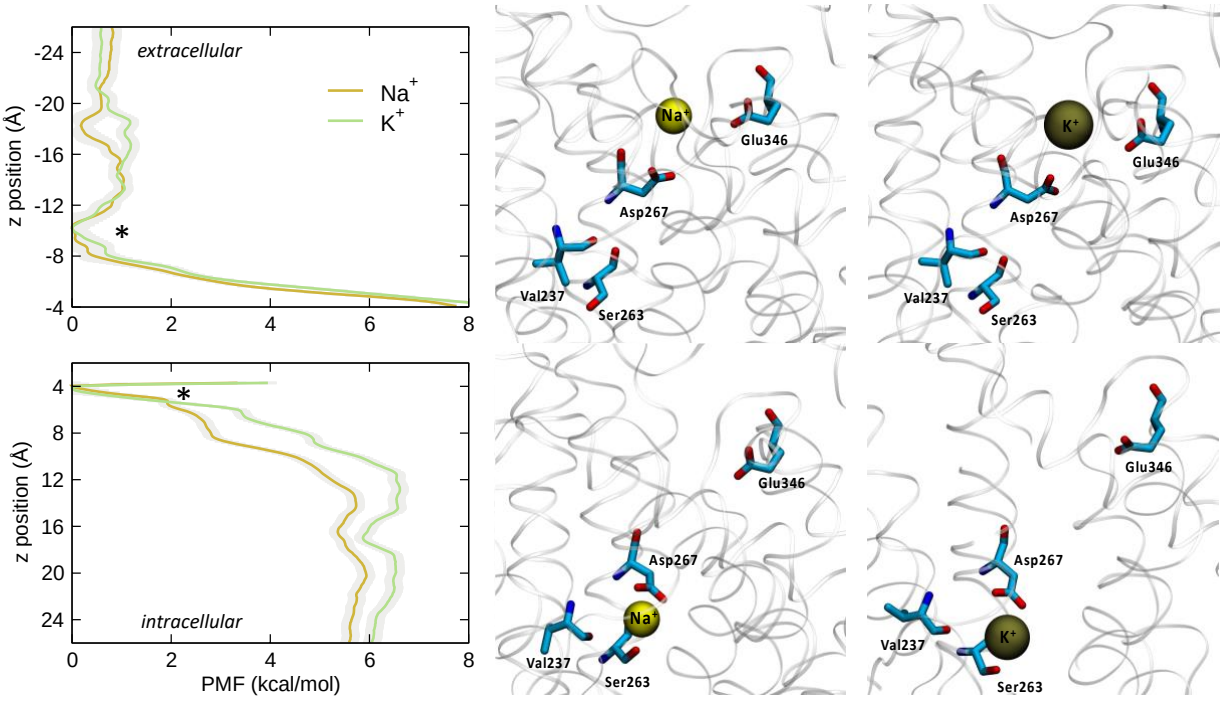

Figure 2. PMF plots of Na^+ (yellow solid line) and K^+ (green dashed line) along the *z*-axis of the outward (top panel) and inward-facing (bottom panel) states of *h*NHE1. Snapshots from the umbrella sampling simulations are showing the coordination of Na^+ (yellow sphere) and K^+ (green sphere) with the residues of *h*NHE1 at the ion-binding site regions where $z = -10$ and 4 Å in the outward and inward-facing states, respectively. Asp267 is facing the periplasm in the outward-

facing state and the cytoplasm in its inward facing state. Error is estimated using bootstrapping analysis.

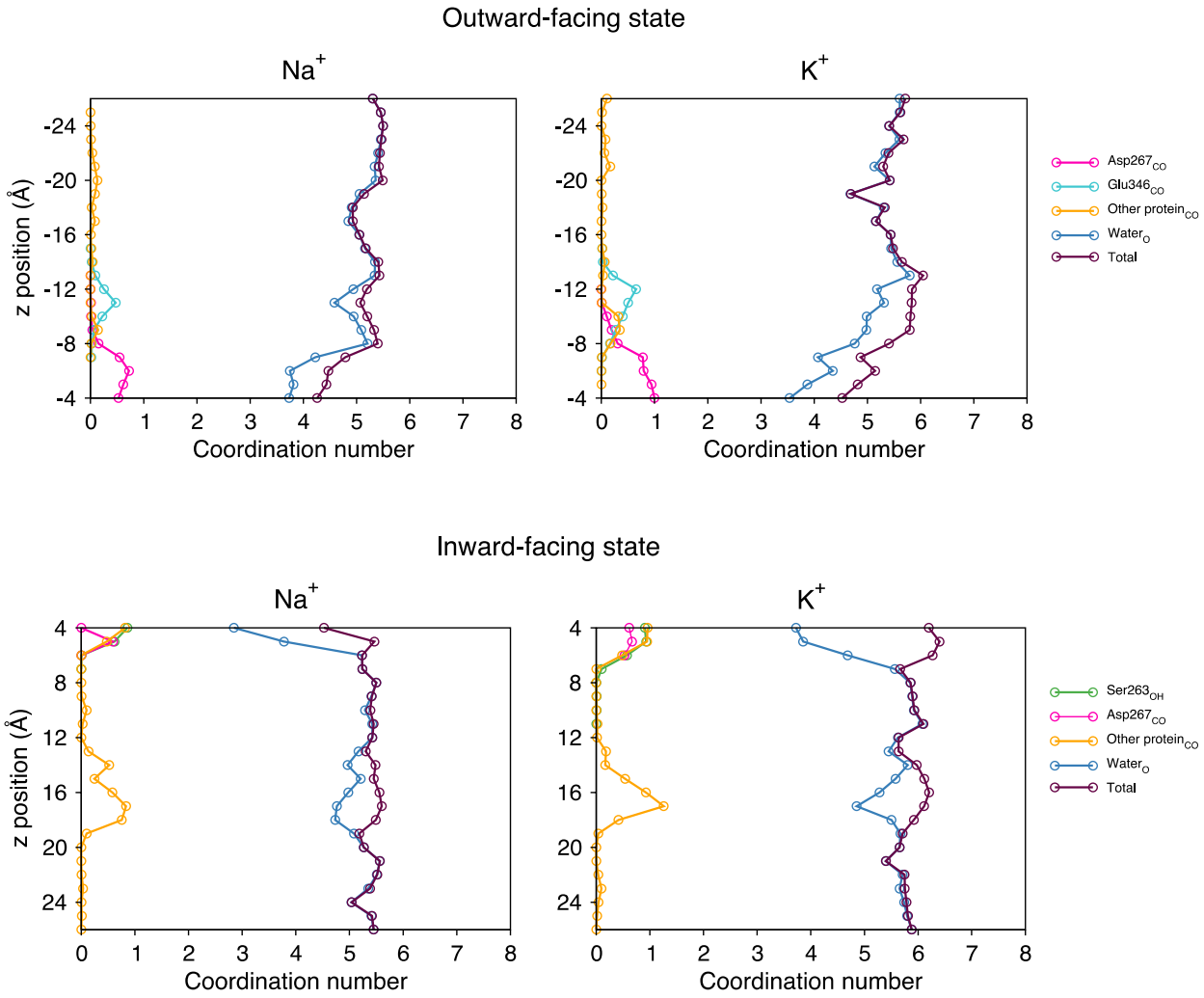

Figure 3. Average number of oxygen atoms (water, backbone carbonyls and side chain hydroxyls) coordinating Na^+ and K^+ along their positions in the pore of the outward (top panel) and inward-facing (bottom panel) states of *h*NHE1. Coordinating oxygen atoms are within 2.8 Å and 3.2 Å from Na^+ and K^+, respectively.

Surprisingly, our FEP calculations didn't show any significant preference for the binding of Na^+ over K^+ to the ion-binding site in the outward or inward-facing states. PMF simulations showed a

slight preference for Na^+ over K^+ in the inward-facing state. It seems that ion binding alone might not be responsible for the observed Na^+ over K^+ selectivity. This is in line with a previous study on the *Ec*NhaA that showed that its binding site is permissive, allowing the binding of several alkali ions and that binding alone is insufficient to account for selectivity.[65] Na^+ binding to the binding site is believed to induce electrostatic changes that trigger conformational changes that lead to Na^+ translocation through the pore.[98] Such conformational changes are beyond the simulation time scale in this work.[38] Cariporide is believed to compete with Na^+ for binding with Asp267 from the extracellular side and inhibit *h*NHE1 activity by blocking the relative sliding movement between the two domains.[34]

Ligands bound to *h*NHE1 maintain key interactions with Asp267 and Glu346

As we are interested in developing amiloride analogues as potential inhibitors for *h*NHE1,[54] we performed MD simulations of six *h*NHE1 inhibitors to study their binding and interactions. These inhibitors are cariporide **1**, amiloride **2**, 5-(*N*,*N*-hexamethylene)amiloride (HMA) **3** and three 6-substituted HMA derivatives; the benzofuranyl **4**, pyrimidinyl **5** and 2-methoxypyrimidinyl **6** analogues.[61] **Table S5** lists their chemical structures and IC_{50} values for *h*NHE1 inhibition as inferred from the whole-cell ΔpH assays.[71, 73] Simulations showed stable protein (**Figure S15**) and ligand (**Figure S16**) RMSDs. RMSF plots revealed high fluctuations of the C_α atoms of residues in the regions comprising the loops and the regions of the assigned TM helices were rigid (**Figure S17**). Throughout the simulations, all inhibitors maintained the key salt bridge interaction between the acylguanidine and the Asp267 side-chain carboxylate as well as hydrogen bonds between the acylguanidine amide nitrogen and the Glu346 side-chain carboxylate (**Figures 4** and **S18**). Our data concluded that the salt bridge interaction between the acylguanidine and Asp267 is aan

important interaction for the binding of amiloride and its analogues. The positively charged acylguanidine group of the inhibitors, which resembles a hydrated Na^+ binds to the ion- binding site and is suggested to compete with extracellular Na^+.[34, 98] Unfortunately, from our simulations, we couldn't discern the reason for the significant loss in potency due to the introduction of a methoxy group in 2-methoxypyrimidinyl **6** (IC_{50} 21.51 µM) when compared to its analogue **5** (IC_{50} 0.397 µM). The molecular mechanisms behind this could be further studied by relative binding free energy calculations.

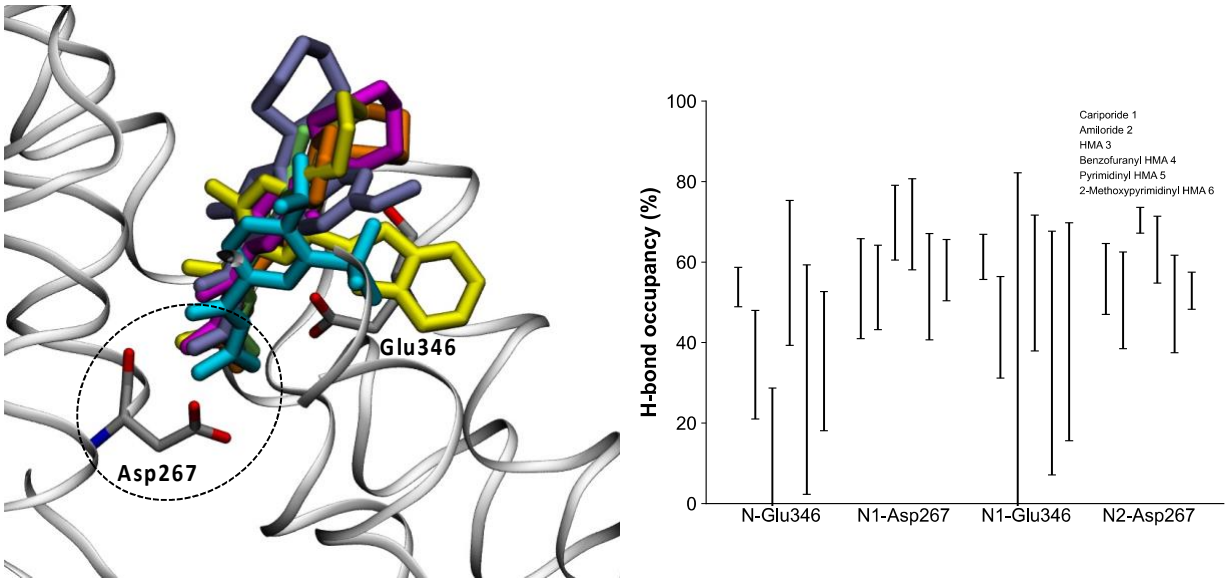

Figure 4. (A) Snapshots from the MD simulations of inhibitors **1** – **6** bound to the *h*NHE1 outward-facing state**.** (B) Mean occupancy (%) of the key hydrogen bond interactions of the inhibitors bound to the outward-facing state of *h*NHE1 along the MD simulations. Error bars represent the standard deviation (see **Table S6** for raw data).

CONCLUSIONS

Our homology model of the *h*NHE1 compares favourably to the recent and long-awaited experimental cryo-EM structure. While all previous models suggested 12 TM segments, ours comprised 13 TM segments matching that of the recent experimental structure. MD simulations of the cryo-EM structure revealed persistent ion binding and unbinding to the experimentally proposed ion-binding residue Asp267. While there is no significant difference in binding free energies for Na^+ or K^+ in the outward and inward-facing states at the ion-binding site, a minor preference was observed in their transporting potential of mean forces. Our work suggests that ion selectivity of *h*NHE1 cannot be explained solely by differences in ion-binding or transporting in the inward and outward-facing states. This can be further investigated for possible ion-dependent induced conformational transitions between the outward and inward-facing states. Cariporide and amiloride-based analogues compete with Na^+ for binding with Asp267 from the extracellular side. They maintain the key salt bridge interaction between their positively charged acylguanidine and Asp267 and thus inhibit *h*NHE1 activity. It is important to maintain this key functional group that resembles a hydrated Na^+ for future development of *h*NHE1 inhibitors.

ASSOCIATED CONTENT

Supporting Information

The Supporting Information is available free of charge at …

Figures S1 and S2 with models of *h*NHE1, Tables S1 and S2 with simulation details, Tables S3 and S4 and Figures S3 – S9 with detailed results on homology models (supplementary section on homology modelling), Table S5 with structures and IC_{50} values of inhibitors, Figures S10− S18 and Table S6 with detailed simulation results on cryo-EM structures (PDF)

Structures of homology models (homology_model_outward_state.pdb, homology_model_inward_state.pdb) (PDB)

Initial structures for ligand bound MD simulations (cariporide.pdb, amiloride.pdb, hma.pdb, benzofuranyl_hma, pyrimidinyl_hma, 2-methoxypyrimidinyl_hma) (PDB)

AUTHOR INFORMATION

Corresponding Author

Haibo Yu – School of Chemistry and Molecular Bioscience, University of Wollongong, Wollongong, NSW 2522, Australia; Molecular Horizons, University of Wollongong, Wollongong, NSW 2522, Australia; orcid.org/0000-0002-1099-2803

E-mail: hyu@uow.edu.au

Authors

Nehad S El Salamouni − School of Chemistry and Molecular Bioscience, University of Wollongong, Wollongong, NSW 2522, Australia; Molecular Horizons, University of Wollongong, Wollongong, NSW 2522, Australia; orcid.org/0000-0001-6856-6332

Benjamin J. Buckley − School of Chemistry and Molecular Bioscience, University of Wollongong, Wollongong, NSW 2522, Australia; Molecular Horizons, University of Wollongong, Wollongong, NSW 2522, Australia, Australia; orcid.org/0000-0002-8346-3371

Richmond Lee − School of Chemistry and Molecular Bioscience, University of Wollongong, Wollongong, NSW 2522, Australia; Molecular Horizons, University of Wollongong, Wollongong, NSW 2522, Australia; orcid.org/0000-0003-1264-4914

Marie Ranson − School of Chemistry and Molecular Bioscience, University of Wollongong, Wollongong, NSW 2522, Australia; Molecular Horizons, University of Wollongong, Wollongong, NSW 2522, Australia; orcid.org/0000-0002-5570-9645

Michael J. Kelso − School of Chemistry and Molecular Bioscience, University of Wollongong, Wollongong, NSW 2522, Australia; Molecular Horizons, University of Wollongong, Wollongong, NSW 2522, Australia; orcid.org/0000-0001-7809-6637

Author Contributions

N.S.E conducted the computational work, analyzed the data and interpreted the results under the directions of H.Y and M.J.K. N.S.E wrote the original manuscript, which was edited and revised by all authors.

Notes

The authors declare no competing financial interest.

ACKNOWLEDGMENTS

This work was funded by an Australian National Health and Medical Research Council (NHMRC) Project Grant (APP1100432) awarded to M.K. and M.R. and a UOW RevITAlise Research Grant Scheme (H.Y. and R.L.). The research was undertaken using resources at the NCI National Facility systems at the Australian National University, provided through the Australian Government National Computational Merit Allocation and Adapter Schemes (project ID v15 and cg98). We would like to thank Prof. Larry Fliegel (University of Alberta) for helpful discussions during the early stages of this work.

REFERENCES

(1) Pedersen, S.; Counillon, L., The SLC9A-C mammalian Na+/H+ exchanger family: molecules, mechanisms, and physiology. *Physiol. Rev.* **2019,** *99* (4), 2015-2113.
(2) Putney, L.; Denker, S.; Barber, D., The changing face of the Na+/H+ exchanger, NHE1: structure, regulation, and cellular actions. *Annu. Rev. Pharmacol. Toxicol.* **2002,** *42* (1), 527-552.
(3) Patiño-Ruiz, M.; Ganea, C.; Călinescu, O., Prokaryotic Na+/H+ exchangers—transport mechanism and essential residues. *Int. J. Mol. Sci.* **2022,** *23* (16), 9156.
(4) Grinstein, S.; Rotin, D.; Mason, M. J., Na+/H+ exchange and growth factor-induced cytosolic pH changes. Role in cellular proliferation. *Biochim. Biophys. Acta* **1989,** *988* (1), 73-97.
(5) Grinstein, S.; Woodside, M.; Sardet, C.; Pouyssegur, J.; Rotin, D., Activation of the Na+/H+ antiporter during cell volume regulation. Evidence for a phosphorylation-independent mechanism. *J. Biol. Chem.* **1992,** *267* (33), 23823-23828.
(6) Fliegel, L., The Na+/H+ exchanger isoform 1. *Int. J. Biochem. Cell Biol.* **2005,** *37* (1), 33-37.
(7) Stock, C.; Schwab, A., Role of the Na+/H+ exchanger NHE1 in cell migration. *Acta Physiol.* **2006,** *187* (1-2), 149-157.
(8) Denker , S. P.; Barber , D. L., Cell migration requires both ion translocation and cytoskeletal anchoring by the Na-H exchanger NHE1. *J. Cell Biol.* **2002,** *159* (6), 1087-1096.
(9) Karmazyn, M., NHE-1: still a viable therapeutic target. *J. Mol. Cell. Cardiol.* **2013,** *61*, 77-82.
(10) Fliegel, L., Regulation of the Na+/H+ exchanger in the healthy and diseased myocardium. *Expert Opin. Ther. Targets* **2009,** *13* (1), 55-68.
(11) Malo, M. E.; Fliegel, L., Physiological role and regulation of the Na+/H+ exchanger. *Can. J. Physiol. Pharmacol.* **2006,** *84* (11), 1081-1095.
(12) Garciandia, A.; López, R.; Tisaire, J.; Arrázola, A.; Fortuño, A.; Bueno, J.; Diez, J., Enhanced Na+-H+ exchanger activity and NHE-1 mRNA expression in lymphocytes from patients with essential hypertension. *Hypertension* **1995,** *25* (3), 356-364.

(13) Bobulescu, I. A.; Di Sole, F.; Moe, O. W., Na+/H+ exchangers: physiology and link to hypertension and organ ischemia. *Curr. Opin. Nephrol. Hypertens.* **2005,** *14* (5), 485-494.
(14) Reshkin, S. J.; Bellizzi, A.; Caldeira, S.; Albarani, V.; Malanchi, I.; Poignee, M.; Alunni-Fabbroni, M.; Casavola, V.; Tommasino, M., Na+/H+ exchanger-dependent intracellular alkalinization is an early event in malignant transformation and plays an essential role in the development of subsequent transformation-associated phenotypes. *FASEB J.* **2000,** *14* (14), 2185-2197.
(15) Amith, S. R.; Vincent, K. M.; Wilkinson, J. M.; Postovit, L. M.; Fliegel, L., Defining the Na+/H+ exchanger NHE1 interactome in triple-negative breast cancer cells. *Cell. Signal.* **2017,** *29*, 69-77.
(16) Cardone, R. A.; Casavola, V.; Reshkin, S. J., The role of disturbed pH dynamics and the Na+/H+ exchanger in metastasis. *Nat. Rev. Cancer* **2005,** *5* (10), 786-795.
(17) Hu, Y.; Lou, J.; Jin, Z.; Yang, X.; Shan, W.; Du, Q.; Liao, Q.; Xu, J.; Xie, R., Advances in research on the regulatory mechanism of NHE1 in tumors (Review). *Oncol. Lett.* **2021,** *21* (4), 273.
(18) Amith, S. R.; Fliegel, L., Regulation of the Na+/H+ exchanger (NHE1) in breast cancer metastasis. *Cancer Res.* **2013,** *73* (4), 1259-1264.
(19) Amith, S. R.; Fong, S.; Baksh, S.; Fliegel, L., Na+/H+ exchange in the tumour microenvironment: does NHE1 drive breast cancer carcinogenesis? *Int. J. Dev. Biol.* **2015,** *59* (7-9), 367-377
(20) Amith, S. R.; Wilkinson, J. M.; Fliegel, L., Na+/H+ exchanger NHE1 regulation modulates metastatic potential and epithelial-mesenchymal transition of triple-negative breast cancer cells. *Oncotarget* **2016,** *7* (16), 21091.
(21) Sanhueza, C.; Araos, J.; Naranjo, L.; Toledo, F.; Beltrán, A. R.; Ramirez, M. A.; Gutierrez, J.; Pardo, F.; Leiva, A.; Sobrevia, L., Sodium/proton exchanger isoform 1 regulates intracellular pH and cell proliferation in human ovarian cancer. *Biochim. Biophys. Acta - Molecular Basis of Disease* **2017,** *1863* (1), 81-91.
(22) Lee, S.; Lee, H.; Yi, K. Y.; Lee, B. H.; Yoo, S.-e.; Lee, K.; Cho, N. S., 4-Substituted (benzo[b]thiophene-2-carbonyl)guanidines as novel Na+/H+ exchanger isoform-1 (NHE-1) inhibitors. *Bioorg. Med. Chem. Lett.* **2005,** *15* (12), 2998-3001.
(23) Hosen, S.; Uddin, M. N.; Xu, Z.; Buckley, B. J.; Perera, C.; Pang, T. C.; Moni, M. A.; Notta, F.; Gallinger, S.; Pirola, R., Metastatic phenotype and immunosuppressive tumour microenvironment in pancreatic ductal adenocarcinoma: Key role of the urokinase plasminogen activator (PLAU). *Front. Immunol.* **2022,** *13*, 1060957.
(24) Kumar, A. A.; Buckley, B. J.; Ranson, M., The urokinase plasminogen activation system in pancreatic cancer: prospective diagnostic and therapeutic targets. *Biomolecules* **2022,** *12* (2), 152.
(25) Fafournoux, P.; Noël, J.; Pouysségur, J., Evidence that Na+/H+ exchanger isoforms NHE1 and NHE3 exist as stable dimers in membranes with a high degree of specificity for homodimers. *J. Biol. Chem.* **1994,** *269* (4), 2589-2596.
(26) Li, X.; Buckley, B.; Stoletov, K.; Jing, Y.; Ranson, M.; Lewis, J. D.; Kelso, M.; Fliegel, L., Roles of the Na+/H+ Exchanger Isoform 1 and Urokinase in Prostate Cancer Cell Migration and Invasion. *Int. J. Mol. Sci.* **2021,** *22* (24), 13263.
(27) Yang, X.; Wang, D.; Dong, W.; Song, Z.; Dou, K., Over-expression of Na+/H+ exchanger 1 and its clinicopathologic significance in hepatocellular carcinoma. *Med. Oncol.* **2010,** *27* (4), 1109-1113.

(28) Mitchell, P., Coupling of phosphorylation to electron and hydrogen transfer by a chemi-osmotic type of mechanism. *Nature* **1961,** *191* (4784), 144-148.
(29) Murer, H.; Hopfer, U.; Kinne, R., Sodium/proton antiport in brush-border-membrane vesicles isolated from rat small intestine and kidney. *Biochem. J.* **1976,** *154* (3), 597-604.
(30) Sardet, C.; Franchi, A.; Pouyssegur, J., Molecular cloning, primary structure, and expression of the human growth factor-activatable Na+ H+ antiporter. *Cell* **1989,** *56* (2), 271-280.
(31) Counillon, L.; Pouyssegur, J.; Reithmeier, R. A., The Na+/H+ exchanger NHE-1 possesses N-and O-linked glycosylation restricted to the first N-terminal extracellular domain. *Biochemistry* **1994,** *33* (34), 10463-10469.
(32) Wakabayashi, S.; Fafournoux, P.; Sardet, C.; Pouysségur, J., The Na+/H+ antiporter cytoplasmic domain mediates growth factor signals and controls "H(+)-sensing". *Proc. Natl. Acad. Sci.* **1992,** *89* (6), 2424-2428.
(33) Koliakos, G.; Paletas, K.; Kaloyianni, M., NHE-1: a molecular target for signalling and cell matrix interactions. *Connect. Tissue Res.* **2008,** *49* (3-4), 157-161.
(34) Dong, Y.; Gao, Y.; Ilie, A.; Kim, D.; Boucher, A.; Li, B.; Zhang, X. C.; Orlowski, J.; Zhao, Y., Structure and mechanism of the human NHE1-CHP1 complex. *Nat. Commun.* **2021,** *12* (1), 3474.
(35) Hunte, C.; Screpanti, E.; Venturi, M.; Rimon, A.; Padan, E.; Michel, H., Structure of a Na+/H+ antiporter and insights into mechanism of action and regulation by pH. *Nature* **2005,** *435* (7046), 1197-1202.
(36) Lee, C.; Kang, H. J.; von Ballmoos, C.; Newstead, S.; Uzdavinys, P.; Dotson, D. L.; Iwata, S.; Beckstein, O.; Cameron, A. D.; Drew, D., A two-domain elevator mechanism for sodium/proton antiport. *Nature* **2013,** *501* (7468), 573-577.
(37) Paulino, C.; Wöhlert, D.; Kapotova, E.; Yildiz, Ö.; Kühlbrandt, W., Structure and transport mechanism of the sodium/proton antiporter MjNhaP1. *eLife* **2014,** *3*, e03583.
(38) Wöhlert, D.; Kühlbrandt, W.; Yildiz, Ö., Structure and substrate ion binding in the sodium/proton antiporter PaNhaP. *eLife* **2014,** *3*, e03579.
(39) Slepkov, E. R.; Rainey, J. K.; Li, X.; Liu, Y.; Cheng, F. J.; Lindhout, D. A.; Sykes, B. D.; Fliegel, L., Structural and functional characterization of transmembrane segment IV of the NHE1 isoform of the Na+/H+ exchanger. *J. Biol. Chem.* **2005,** *280* (18), 17863-17872.
(40) Tzeng, J.; Lee, B. L.; Sykes, B. D.; Fliegel, L., Structural and functional analysis of transmembrane segment VI of the NHE1 isoform of the Na+/H+ exchanger. *J. Biol. Chem.* **2010,** *285* (47), 36656-36665.
(41) Ding, J.; Rainey, J. K.; Xu, C.; Sykes, B. D.; Fliegel, L., Structural and functional characterization of transmembrane segment VII of the Na+/H+ exchanger isoform 1. *J. Biol. Chem.* **2006,** *281* (40), 29817-29829.
(42) Alves, C.; Lee, B. L.; Sykes, B. D.; Fliegel, L., Structural and functional analysis of the transmembrane segment pair VI and VII of the NHE1 isoform of the Na+/H+ exchanger. *Biochemistry* **2014,** *53* (22), 3658-3670.
(43) Reddy, T.; Ding, J.; Li, X.; Sykes, B. D.; Rainey, J. K.; Fliegel, L., Structural and functional characterization of transmembrane segment IX of the NHE1 isoform of the Na+/H+ exchanger. *J. Biol. Chem.* **2008,** *283* (32), 22018-22030.
(44) Lee, B. L.; Li, X.; Liu, Y.; Sykes, B. D.; Fliegel, L., Structural and functional analysis of transmembrane XI of the NHE1 isoform of the Na+/H+ exchanger. *J. Biol. Chem.* **2009,** *284* (17), 11546-11556.

(45) Wong, K. Y.; McKay, R.; Liu, Y.; Towle, K.; Elloumi, Y.; Li, X.; Quan, S.; Dutta, D.; Sykes, B. D.; Fliegel, L., Diverse residues of intracellular loop 5 of the Na+/H+ exchanger modulate proton sensing, expression, activity and targeting. *Biochim. Biophys. Acta Biomembr.* **2019,** *1861* (1), 191-200.
(46) Wakabayashi, S.; Pang, T.; Su, X.; Shigekawa, M., A novel topology model of the human Na+/H+ exchanger isoform 1. *J. Biol. Chem.* **2000,** *275* (11), 7942-7949.
(47) Landau, M.; Herz, K.; Padan, E.; Ben-Tal, N., Model structure of the Na+/H+ exchanger 1 (NHE1) functional and clinical implications. *J. Biol. Chem.* **2007,** *282* (52), 37854-37863.
(48) Nygaard, E. B.; Lagerstedt, J. O.; Bjerre, G.; Shi, B.; Budamagunta, M.; Poulsen, K. A.; Meinild, S.; Rigor, R. R.; Voss, J. C.; Cala, P. M., Structural modeling and electron paramagnetic resonance spectroscopy of the human Na+/H+ exchanger isoform 1, NHE1. *J. Biol. Chem.* **2011,** *286* (1), 634-648.
(49) Dutta, D.; Fliegel, L., Molecular modeling and inhibitor docking analysis of the Na+/H+ exchanger isoform one. *Biochem. Cell Biol.* **2018,** *97* (3), 333-343.
(50) Kyte, J.; Doolittle, R. F., A simple method for displaying the hydropathic character of a protein. *J. Mol. Biol.* **1982,** *157* (1), 105-132.
(51) Counillon, L.; Franchi, A.; Pouysségur, J., A point mutation of the Na+/H+ exchanger gene (NHE1) and amplification of the mutated allele confer amiloride resistance upon chronic acidosis. *Proc. Natl. Acad. Sci. U.S.A.* **1993,** *90* (10), 4508-4512.
(52) Harguindey, S.; Arranz, J. L.; Polo Orozco, J. D.; Rauch, C.; Fais, S.; Cardone, R. A.; Reshkin, S. J., Cariporide and other new and powerful NHE1 inhibitors as potentially selective anticancer drugs–an integral molecular/biochemical/metabolic/clinical approach after one hundred years of cancer research. *J. Transl. Med.* **2013,** *11*, 1-17.
(53) Rolver, M. G.; Elingaard-Larsen, L. O.; Andersen, A. P.; Counillon, L.; Pedersen, S. F., Pyrazine ring-based Na+/H+ exchanger (NHE) inhibitors potently inhibit cancer cell growth in 3D culture, independent of NHE1. *Sci. Rep.* **2020,** *10* (1), 1-17.
(54) El Salamouni, N. S.; Buckley, B. J.; Ranson, M.; Kelso, M. J.; Yu, H., Urokinase plasminogen activator as an anti-metastasis target: inhibitor design principles, recent amiloride derivatives, and issues with human/mouse species selectivity. *Biophys. Rev.* **2022**, 1-25.
(55) Wakabayashi, S.; Shigekawa, M.; Pouyssegur, J., Molecular physiology of vertebrate Na+/H+ exchangers. *Physiol. Rev.* **1997,** *77* (1), 51-74.
(56) Vigne, P.; Frelin, C.; Lazdunski, M., The amiloride-sensitive Na+/H+ exchange system in skeletal muscle cells in culture. *J. Biol. Chem.* **1982,** *257* (16), 9394-9400.
(57) Harris, C.; Fliegel, L., Amiloride and the Na (+)/H (+) exchanger protein: mechanism and significance of inhibition of the Na (+)/H (+) exchanger. *Int. J. Mol. Med.* **1999,** *3* (3), 315.
(58) Counillon, L.; Noël, J.; Reithmeier, R. A.; Pouysségur, J., Random mutagenesis reveals a novel site involved in inhibitor interaction within the fourth transmembrane segment of the Na+/H+ exchanger-1. *Biochemistry* **1997,** *36* (10), 2951-2959.
(59) Li, X.; Kim, J.; Yang, J.; Dutta, D.; Fliegel, L., Characterization of modeled inhibitory binding sites on isoform one of the Na+/H+ exchanger. *Biochim. Biophys. Acta Biomembr.* **2021,** *1863* (9), 183648.
(60) Zhuang, Y. X.; Cragoe Jr, E. J.; Shaikewitz, T.; Glaser, L.; Cassel, D., Characterization of potent sodium/proton exchange inhibitors from the amiloride series in A431 cells. *Biochemistry* **1984,** *23* (19), 4481-4488.

(61) Buckley, B. J.; Kumar, A.; Aboelela, A.; Bujaroski, R. S.; Li, X.; Majed, H.; Fliegel, L.; Ranson, M.; Kelso, M. J., Screening of 5-and 6-substituted amiloride libraries identifies dual-uPA/NHE1 active and single target-selective inhibitors. *Int. J. Mol. Sci.* **2021,** *22* (6), 2999.
(62) Warnau, J.; Wöhlert, D.; Okazaki, K.-i.; Yildiz, O. z.; Gamiz-Hernandez, A. P.; Kaila, V. R.; Kühlbrandt, W.; Hummer, G., Ion binding and selectivity of the Na+/H+ antiporter MjNhaP1 from experiment and simulation. *J. Phys. Chem. B* **2019,** *124* (2), 336-344.
(63) Schuldiner, S.; Fishkes, H., Sodium-proton antiport in isolated membrane vesicles of Escherichia coli. *Biochemistry* **1978,** *17* (4), 706-711.
(64) Arkin, I. T.; Xu, H.; Jensen, M. Ø.; Arbely, E.; Bennett, E. R.; Bowers, K. J.; Chow, E.; Dror, R. O.; Eastwood, M. P.; Flitman-Tene, R., Mechanism of Na+/H+ antiporting. *Science* **2007,** *317* (5839), 799-803.
(65) Alhadeff, R.; Ganoth, A.; Krugliak, M.; Arkin, I. T., Promiscuous binding in a selective protein: the bacterial Na+/H+ antiporter. *PLoS One* **2011,** *6* (10), e25182.
(66) Brett, C. L.; Donowitz, M.; Rao, R., Evolutionary origins of eukaryotic sodium/proton exchangers. *Am. J. Physiol. Cell Physiol.* **2005,** *288* (2), C223-C239.
(67) Zhang, H.-X.; Blumwald, E., Transgenic salt-tolerant tomato plants accumulate salt in foliage but not in fruit. *Nat. Biotechnol.* **2001,** *19* (8), 765-768.
(68) Gierth, M.; Mäser, P., Potassium transporters in plants – Involvement in K+ acquisition, redistribution and homeostasis. *FEBS Lett.* **2007,** *581* (12), 2348-2356.
(69) Nakamura, N.; Tanaka, S.; Teko, Y.; Mitsui, K.; Kanazawa, H., Four Na+/H+ exchanger isoforms are distributed to Golgi and post-Golgi compartments and are involved in organelle pH regulation. *J. Biol. Chem.* **2005,** *280* (2), 1561-1572.
(70) S El Salamouni, N.; Buckley, B. J.; Jiang, L.; Huang, M.; Ranson, M.; Kelso, M. J.; Yu, H., Disruption of water networks is the cause of human/mouse species selectivity in urokinase plasminogen activator (uPA) inhibitors derived from hexamethylene amiloride (HMA). *J. Med. Chem.* **2021,** *65* (3), 1933-1945.
(71) Buckley, B. J.; Aboelela, A.; Minaei, E.; Jiang, L. X.; Xu, Z.; Ali, U.; Fildes, K.; Cheung, C.-Y.; Cook, S. M.; Johnson, D. C.; Bachovchin, D. A.; Cook, G. M.; Apte, M.; Huang, M.; Ranson, M.; Kelso, M. J., 6-Substituted Hexamethylene Amiloride (HMA) Derivatives as Potent and Selective Inhibitors of the Human Urokinase Plasminogen Activator for Use in Cancer. *J. Med. Chem.* **2018,** *61* (18), 8299-8320.
(72) Matthews, H.; Ranson, M.; Kelso, M. J., Anti-tumour/metastasis effects of the potassium-sparing diuretic amiloride: An orally active anti-cancer drug waiting for its call-of-duty? *Int. J. Cancer* **2011,** *129* (9), 2051-2061.
(73) Buckley, B. J.; Aboelela, A.; Majed, H.; Bujaroski, R. S.; White, K. L.; Powell, A. K.; Wang, W.; Katneni, K.; Saunders, J.; Shackleford, D. M.; Charman, S. A.; Cook, G. M.; Kelso, M. J.; Ranson, M., Systematic evaluation of structure–property relationships and pharmacokinetics in 6-(hetero)aryl-substituted matched pair analogs of amiloride and 5-(N,N-hexamethylene)amiloride. *Bioorg. Med. Chem.* **2021,** *37*, 116116.
(74) Lomize, M. A.; Lomize, A. L.; Pogozheva, I. D.; Mosberg, H. I., OPM: orientations of proteins in membranes database. *Bioinformatics* **2006,** *22* (5), 623-625.
(75) Jo, S.; Kim, T.; Iyer, V. G.; Im, W., CHARMM-GUI: A web-based graphical user interface for CHARMM. *J. Comput. Chem.* **2008,** *29* (11), 1859-1865.
(76) Brooks, B. R.; Brooks III, C. L.; Mackerell Jr., A. D.; Nilsson, L.; Petrella, R. J.; Roux, B.; Won, Y.; Archontis, G.; Bartels, C.; Boresch, S.; Caflisch, A.; Caves, L.; Cui, Q.; Dinner, A. R.; Feig, M.; Fischer, S.; Gao, J.; Hodoscek, M.; Im, W.; Kuczera, K.; Lazaridis, T.; Ma,

J.; Ovchinnikov, V.; Paci, E.; Pastor, R. W.; Post, C. B.; Pu, J. Z.; Schaefer, M.; Tidor, B.; Venable, R. M.; Woodcock, H. L.; Wu, X.; Yang, W.; York, D. M.; Karplus, M., CHARMM: The biomolecular simulation program. *J. Comput. Chem.* **2009,** *30* (10), 1545-1614.
(77) Lee, J.; Cheng, X.; Swails, J. M.; Yeom, M. S.; Eastman, P. K.; Lemkul, J. A.; Wei, S.; Buckner, J.; Jeong, J. C.; Qi, Y.; Jo, S.; Pande, V. S.; Case, D. A.; Brooks, C. L.; MacKerell, A. D.; Klauda, J. B.; Im, W., CHARMM-GUI Input Generator for NAMD, GROMACS, AMBER, OpenMM, and CHARMM/OpenMM Simulations Using the CHARMM36 Additive Force Field. *J. Chem. Theory Comput.* **2016,** *12* (1), 405-413.
(78) Phillips, J. C.; Braun, R.; Wang, W.; Gumbart, J.; Tajkhorshid, E.; Villa, E.; Chipot, C.; Skeel, R. D.; Kalé, L.; Schulten, K., Scalable molecular dynamics with NAMD. *J. Comput. Chem.* **2005,** *26* (16), 1781-1802.
(79) Klauda, J. B.; Venable, R. M.; Freites, J. A.; O'Connor, J. W.; Tobias, D. J.; Mondragon-Ramirez, C.; Vorobyov, I.; MacKerell Jr, A. D.; Pastor, R. W., Update of the CHARMM all-atom additive force field for lipids: validation on six lipid types. *J. Phys. Chem. B* **2010,** *114* (23), 7830-7843.
(80) Huang, J.; MacKerell Jr, A. D., CHARMM36 all-atom additive protein force field: Validation based on comparison to NMR data. *J. Comput. Chem.* **2013,** *34* (25), 2135-2145.
(81) Vanommeslaeghe, K.; Hatcher, E.; Acharya, C.; Kundu, S.; Zhong, S.; Shim, J.; Darian, E.; Guvench, O.; Lopes, P.; Vorobyov, I., CHARMM general force field: A force field for drug-like molecules compatible with the CHARMM all-atom additive biological force fields. *J. Comput. Chem.* **2010,** *31* (4), 671-690.
(82) Olsson, M. H. M.; Søndergaard, C. R.; Rostkowski, M.; Jensen, J. H., PROPKA3: Consistent Treatment of Internal and Surface Residues in Empirical pKa Predictions. *J. Chem. Theory Comput.* **2011,** *7* (2), 525-537.
(83) Miyamoto, S.; Kollman, P. A., Settle: An analytical version of the SHAKE and RATTLE algorithm for rigid water models. *J. Comput. Chem.* **1992,** *13* (8), 952-962.
(84) Humphrey, W.; Dalke, A.; Schulten, K., VMD: Visual molecular dynamics. *J. Mol. Graph.* **1996,** *14* (1), 33-38.
(85) Smart, O. S.; Neduvelil, J. G.; Wang, X.; Wallace, B. A.; Sansom, M. S. P., HOLE: A program for the analysis of the pore dimensions of ion channel structural models. *J. Mol. Graph.* **1996,** *14* (6), 354-360.
(86) Grossfield, A., "WHAM: the weighted histogram analysis method", http://membrane.urmc.rochester.edu/wordpress/?page_id=126
(87) Liu, P.; Dehez, F.; Cai, W.; Chipot, C., A Toolkit for the Analysis of Free-Energy Perturbation Calculations. *J. Chem. Theory Comput.* **2012,** *8* (8), 2606-2616.
(88) Bennett, C. H., Efficient estimation of free energy differences from Monte Carlo data. *J. Comput. Phys.* **1976,** *22* (2), 245-268.
(89) Trott, O.; Olson, A. J., AutoDock Vina: improving the speed and accuracy of docking with a new scoring function, efficient optimization, and multithreading. *J. Comput. Chem.* **2010,** *31* (2), 455-461.
(90) Eberhardt, J.; Santos-Martins, D.; Tillack, A. F.; Forli, S., AutoDock Vina 1.2.0: New Docking Methods, Expanded Force Field, and Python Bindings. *J. Chem. Inf. Model.* **2021,** *61* (8), 3891-3898.
(91) Hanwell, M. D.; Curtis, D. E.; Lonie, D. C.; Vandermeersch, T.; Zurek, E.; Hutchison, G. R., Avogadro: an advanced semantic chemical editor, visualization, and analysis platform. *J. Cheminformatics* **2012,** *4* (1), 17.

(92) Sanner, M. F., Python: a programming language for software integration and development. *J. Mol. Graph. Model.* **1999,** *17* (1), 57-61.
(93) Morris, G. M.; Huey, R.; Lindstrom, W.; Sanner, M. F.; Belew, R. K.; Goodsell, D. S.; Olson, A. J., AutoDock4 and AutoDockTools4: Automated docking with selective receptor flexibility. *J. Comput. Chem.* **2009,** *30* (16), 2785-2791.
(94) Mirdita, M.; Schütze, K.; Moriwaki, Y.; Heo, L.; Ovchinnikov, S.; Steinegger, M., ColabFold: making protein folding accessible to all. *Nat. Methods* **2022,** *19* (6), 679-682.
(95) Jumper, J.; Evans, R.; Pritzel, A.; Green, T.; Figurnov, M.; Ronneberger, O.; Tunyasuvunakool, K.; Bates, R.; Žídek, A.; Potapenko, A.; Bridgland, A.; Meyer, C.; Kohl, S. A. A.; Ballard, A. J.; Cowie, A.; Romera-Paredes, B.; Nikolov, S.; Jain, R.; Adler, J.; Back, T.; Petersen, S.; Reiman, D.; Clancy, E.; Zielinski, M.; Steinegger, M.; Pacholska, M.; Berghammer, T.; Bodenstein, S.; Silver, D.; Vinyals, O.; Senior, A. W.; Kavukcuoglu, K.; Kohli, P.; Hassabis, D., Highly accurate protein structure prediction with AlphaFold. *Nature* **2021,** *596* (7873), 583-589.
(96) Liu, Y.; Basu, A.; Li, X.; Fliegel, L., Topological analysis of the Na+/H+ exchanger. *Biochim. Biophys. Acta Biomembr.* **2015,** *1848* (10), 2385-2393.
(97) Noël, J.; Germain, D.; Vadnais, J., Glutamate 346 of human Na+− H+ exchanger NHE1 is crucial for modulating both the affinity for Na+ and the interaction with amiloride derivatives. *Biochemistry* **2003,** *42* (51), 15361-15368.
(98) Poet, M.; Doyen, D.; Van Obberghen, E.; Jarretou, G.; Bouret, Y.; Counillon, L., How Does Our Knowledge on the Na+/H+ Exchanger NHE1 Obtained by Biochemical and Molecular Analyses Keep up With Its Recent Structure Determination? *Front. Physiol.* **2022,** *13*.

For Table of Contents Only